A levelset based method for segmenting the heart in 3D+T gated SPECT images

Arnaud Charnoz, Diane Lingrand, Johan Montagnat

A levelset based method for segmenting the heart in 3D+T gated SPECT images.

Arnaud Charnoz[1], Diane Lingrand[1] and Johan Montagnat[2]

[1] CReATIVe, I3S, CNRS/UNSA
B.P.121 - F06903 Sophia Antipolis Cédex - FRANCE
lingrand@i3s.unice.fr
[2] Creatis, CNRS/INSA Lyon
F69621 Villeurbanne Cédex - FRANCE
johan@creatis.insa-lyon.fr

Abstract. Levelset methods were introduced in medical images segmentation by Malladi *et al* in 1995. In this paper, we propose several improvements of the original method to speed up the algorithm convergence and to improve the quality of the segmentation in the case of cardiac gated SPECT images.
We studied several evolution criterions, taking into account the dynamic property of heart image sequences. For each step of the segmentation algorithm, we have compared different solutions in order to both reduce time and improve quality.
We have developed a modular segmentation tool with 3D+T visualization capabilities to experiment the proposed solutions and tune the algorithm parameters. We show segmentation results on both simulated and real SPECT images.

1 Motivations

Cardiovascular pathologies are the first cause of mortality in industrialized countries. Functional imaging of the heart such as gated SPECT images provide low invasive inspection methods useful for cardiac diagnosis. However, high noise level and low resolution make these images difficult to interpret. Moreover, the dynamic properties of 3D heart image sequences make manual analysis of the images extremely tedious.

In this paper, we propose an automated segmentation method of the heart boundaries based on the levelset method. The resulting models can be used for quantitative dynamic parameters computation useful for medical diagnosis such as the left ventricle volume variations or walls thickness variations. These parameters allow to compute precise estimates of well established clinical indicators such as the ejection fraction. Combining the SPECT intensity information with the model geometry allows to precisely locate necrosed myocardial area, and estimate the tissue viability.

In the following sections we focus on the first step of this process which is the segmentation. Making the segmentation automatic in SPECT images is known

to be a hard problem due to the lack of information (low resolution), blurred boundaries, high noise level, low contrast, and the need for reliable results.

We use a model driven approach in order to segment the heart. Different geometrical models exist (see [10] for a survey). The original model-based segmentation methods were 2D explicit contours [8] later on extended to surfaces in 3D [15, 3]. The levelset method is an alternative implicit surface representation due to Osher and Sethian [11] and Caselles [1]. It has been introduced for segmenting medical images by Malladi and Sethian [9].

Most shape recognition algorithms need to know the topology of objects to recover. The levelset method allows to perform topology changes during the segmentation process without introducing additional complexity. It has been widely used in segmentation [2, 4, 12, 7, 5, 6].

2 The levelset method for segmentation

In the levelset method, the model C is implicitly defined as the zero levelset of a higher dimension function u. Starting from a given shape C_0, the model is able to evolve toward the shape of the object to segment, according to the first order evolution law:

$$\frac{\partial C}{\partial t} = F\vec{\mathbf{N}} = (F_{int} + F_{ext})\vec{\mathbf{N}} \tag{1}$$

with F the force applied on the surface and $\vec{\mathbf{N}}$ the surface normal vector. This force may be decomposed into two components:

- an internal component F_{int}, enforcing a regularity constraint over the surface
- an external component, F_{ext}, taking into account the image to enforce the convergence of the model shape toward the data.

For simplicity, we will explain the levelset approach in case of 2D images. Given an initial contour C_0, the levelset function is $u(x, y) = d((x, y), C_0)$ where d is a signed distance (see figure 1). The initial contour is indeed defined as $C = \{(x, y)|u(x, y) = 0\}$. u is therefore represented as a distance map. Outside the contour, map values are positive. Inside, they are negative.

The level set method shows that the model evolution (equation 1) corresponds to an evolution of the distance map satisfying ([9]):

$$\frac{\partial u}{\partial t} = F \left\|\nabla u\right\| = (F_{int} + F_{ext}) \left\|\nabla u\right\| \tag{2}$$

where $u(x, y, t)$ is the evolutive distance map. This equation is only valid at the model location. As a consequence, the distance map property of u will not be preserved. In order to cope with this problem, we need to reinitialize u periodically so that it corresponds to a distance map, *i.e.* to constrain $\|\nabla u\| = 1$.

The level set formulation extends straight forward in 3D with a higher dimension distance map. We can therefore consider surface model for 3D and 3D+T images segmentation. Equation 2 is discretized using an explicit scheme for numerical implementation.

The segmentation algorithms steps are:

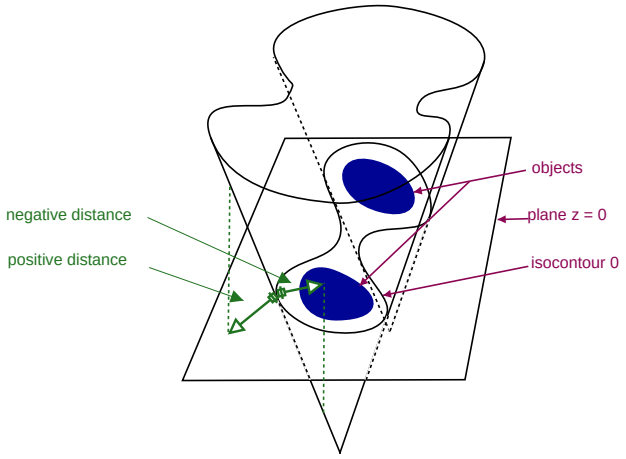

Fig. 1. Distance map u, in dimension 2

Initialization: the initial location of the surface
Loop:
Compute the forces: defined by a criterion
Make the distance map evolve: using equation 2
Reinitialize the distance map: in order to enforce $\|\nabla u\| = 1$.
Convergence: iterate until the algorithm converges (need a stop criterion)

In the following sections, we study each of these steps in order to optimize the segmentation algorithm. We use synthetic data (with or without white noise) made from simple geometric forms or more realistic forms (shape similar to the heart left ventricle) for experiments. We have also used simulated images by the MCAT method [13] and real SPECT data provided by the Pr J. Darcourt of the Pasteur hospital (Nice, France).

3 Initialization

A basic idea for initialization is to take a sphere centered in the volume with a diameter equal to half image dimension. However, this naive approach initializes the model far from the actual object boundaries and the convergence time is long.

The segmentation process time has been decreased by using simple image processing techniques to obtain a closer approximation of the object. The image is first filtered with a Gaussian kernel in order to reduce noise. The mean and variance of image intensity are estimated and a threshold is computed as the sum of these two parameters, in order to eliminate a large part of the background. Thereafter, a morphomathematic opening operation is performed, using this threshold, in order to eliminate small objects due to noise and fuse close components. We extract the surface splitting the resulting binary image in order

to initialize the distance map (see section 5). A similar approach was proposed for the balloon model by Cohen [3].

4 Evolution criterions and parameters

Most evolution criterions proposed in levelset-based segmentation methods are spatial [7]. In the case of dynamic images, they only allow to segment each volume independently of the others. The first criterion that we implemented uses only intensity information. It makes the hypothesis that the image is composed of a uniform intensity region (the object to segment) and a uniform background:

$$\begin{cases} \dfrac{\partial u}{\partial t} = \left(4\,(I-\mu_{int})^2 - (I-\mu_{out})^2 + \lambda\kappa\right)\ \|\nabla u\| \\ \text{with: } \kappa \text{ the curvature,} \\ \qquad \mu_{out} \text{ mean of image external part,} \\ \qquad \mu_{int} \text{ mean of image internal part,} \\ \qquad \text{and } I \text{ image intensity.} \end{cases} \tag{3}$$

This approximation is only roughly valid for SPECT images due to the image noise, the inhomogeneity of the heart and the perfusion deficiencies causing signal drops.

A more elaborated criterion uses both information on intensity and variance of intensity allowing the segmentation of non uniform regions (textured region).

$$\begin{cases} \dfrac{\partial u}{\partial t} = \Big(2\,log(1+\sigma_{int}^2) - log(1+\sigma_{out}^2) \\ \qquad + 2\,\dfrac{(I-\mu_{int})^2-\sigma_{int}^2}{1+\sigma_{int}^2} - \dfrac{(I-\mu_{out})^2-\sigma_{out}^2}{1+\sigma_{out}^2} + \lambda\kappa\Big)\ \|\nabla u\| \\ \text{with: } \kappa \text{ the curvature,} \\ \qquad \mu_{out} \text{ mean of image external part,} \\ \qquad \mu_{int} \text{ mean of image internal part,} \\ \qquad \sigma_{out} \text{ variance of image external part,} \\ \qquad \sigma_{int} \text{ variance of image internal part,} \\ \qquad \text{and } I \text{ image intensity} \end{cases} \tag{4}$$

Equation 5 presents a spatial and temporal criterion [5]. Let I_n represent the image at instant n. The whole sequence is used in order to filter noise and determine the mean background intensity (B):

$$\begin{cases} \dfrac{\partial u_n}{\partial t} = \left(2\,(I_n - \mu_{int_n})^2 - (B-I_n)^2 + \lambda\kappa_n\right)\ \|\nabla u_n\| \\ \text{with: } \kappa_n \text{ the curvature,} \\ \qquad B \text{ the whole sequence mean background intensity,} \\ \qquad \mu_{int_n} \text{ mean of image n internal part,} \\ \qquad \text{and } I_n \text{ image n intensity.} \end{cases} \tag{5}$$

4.1 Influence of the curvature

Using the evolution criterion 3, different weights λ of the curvature have been experimented. The figure 2 shows that for segmentation quality and segmentation time, we need to find a compromise for the λ value.

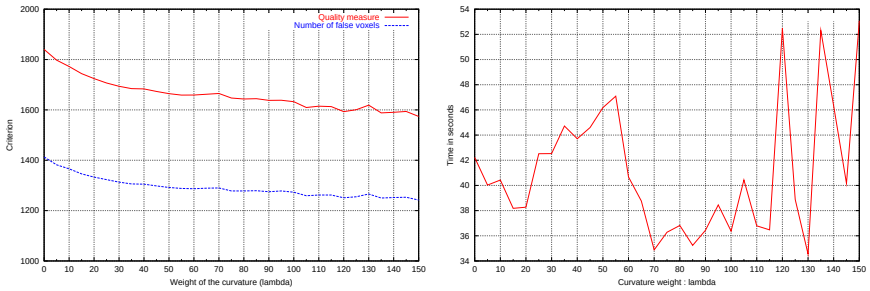

Fig. 2. On the left: evaluation of the quality on the final segmentation for different values of λ. We observe that the larger the curvature weight is, the better the final segmentation is. On the right: segmentation time. For large values of λ, the numerical scheme is unstable. A good compromise is to take a λ value around 100.

4.2 Do we need to recompute the distance map gradient $\|\nabla u\|$?

The distance map gradient $\|\nabla u\|$ is used in the evolution equation 2. If the distance map is a real distance map or if we reinitialize it often, $\|\nabla u\| = 1$ and we do not need to compute it. However, frequent reinitializations are costly.

If we do not reinitialize u frequently, the distance map is false as soon as we update u according to the evolution equation. We observed that the levelset surface becomes sharp and the gradient is high near the isolevel 0. The pixels need a greater force to move from outside to inside the object (and conversely).

A naive approach would consist in introducing the computed value of the gradient into the evolution equation. However, we observed that this quickly makes the explicit numerical scheme unstable. A diminution of the time step is then needed at the cost of an increased convergence time.

It appears that using $\|\nabla u\| = 1$ leads to a more stable algorithm and the distance map only need to be periodically reinitialized.

5 Reinitialization

As seen before, the equation 5 is only true at the model location. This is illustrated in figure 3. In order to preserve the distance map, we need to reinitialize it regularly, every n iterations.

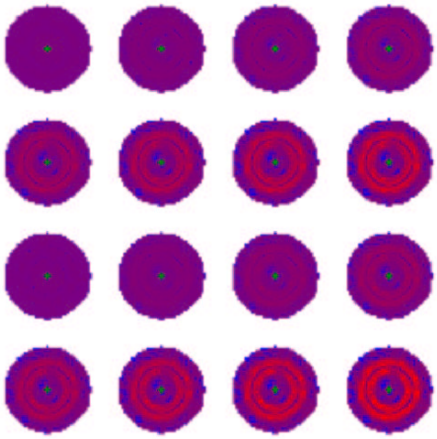

Fig. 3. Evolution of the distance map gradient in the model neighborhood during the segmentation of a synthetic ventricle. The reinitialization is made every 8 iterations. From left to right and top to bottom, we show the 16th first iterations. The blue color corresponds to a gradient value 0, the purple 1 and the red 10, which is the maximum value. The other colors are interpolated from these values.

5.1 Classical Reinitialization

Usually, the distance map is reinitialized using the Sussman *et al* [14] equation:

$$\frac{\partial u}{\partial t} = \text{sign}(u) \times (1 - \|\nabla u\|) \quad \text{where} : \begin{array}{l} \text{if } u < 1, \text{sign}(u) = -1 \\ \text{else if } -1 < u < 1, \text{sign}(u) = |u| \\ \text{else sign}(u) = 1 \end{array} \tag{6}$$

The withdraw of this method is the computation cost. It can be limited using the narrow band method [9]. But is is even more efficient to proceed to a faster reinitialization that is presented in the following section.

5.2 Fast reinitialization

This method involves 2 steps. The first step cuts the distance map just around the model: using 8-connexity in 2D or 26-connexity in 3D, we preserve only pixels or voxels that have a neighbor with an opposite sign in the distance map values. The second step expands this to all the distance map: we begin with distance map values around the edges and propagate the values using distances.

In this case, we reduce the computation cost without reducing the segmentation quality. We can also restrict the reinitialization to a narrow band around the model, but the gain is not as important as in the case of classical reinitialization: distances greater than the narrow band size are not computed and voxels outside the narrow band are assigned a constant upper value.

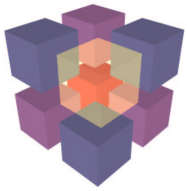

Distances values with respect to the yellow transparent voxel: the blue voxels are at distance 1, the purple $\sqrt{2}$ and the red $\sqrt{3}$.

6 Stopping the segmentation process

We studied several stop conditions: the variation of the surface, the variation of the volume, and the variations of energy criterions. The two first criterions are necessary but not sufficient (when the model converges, its surface and volume are constant). The last one is sufficient (the equation evolution corresponds to a minimization of the model energy with a gradient descent method). However, computing the model volume or surface is much cheaper than computing its energy, and it is very unlikely that the model will evolve significantly for several iterations while its surface and its volume remain constant. Therefore, we used surface and volume variation as stop conditions as well.

We observe periodic oscillations (see figure 4) due to the variation of energy which is caused by the distance map reinitializations: after each reinitialization the distance map is flatten, the surface encounters less resistive gradients, and evolves more than before reinitialization (when we need larger forces to move).

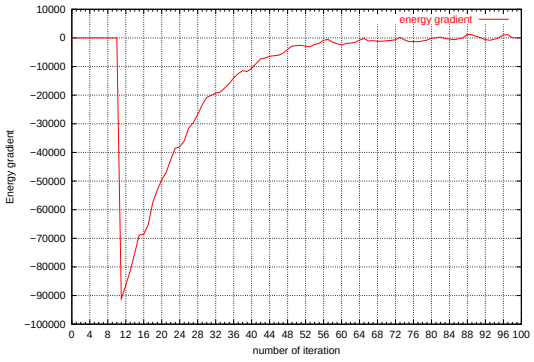

Fig. 4. Energy variation during the segmentation process, using reinitialization every 8 steps. We observe oscillations corresponding to the reinitialization frequency.

7 Experiments

We present in figures 5, 7 and 6 the result of the segmentation of a real SPECT image of the heart left ventricle. The sequence is composed by 8 frames of dimension 64x64x28 voxels. Each voxel has a dimension of 2.5x2.5x5 mm^3. When the heart muscle relaxes (diastole), the contrast between muscle intensity and background decreases. On contrary, the contrast is better when the muscle contracts (systole).

Due to this low contrast in diastole images, a small portion of the right ventricle is also segmented in frames 4 to 7 using criterion 3 or 4 (figures 5 and 7). Spatial criterions fail to take into account image intensity variations along the sequence. Using criterion 5 improves the segmentation by taking into account the intensity variation of the ventricle in the whole sequence (see figure 6). We could further improve this result by taking into account the fact that the myocardium is hardly compressible and that the model volume should be constant in all time frames.

Fig. 5. From left to right and top to bottom, segmentation results from frame 0 to frame 7 of the cardiac sequence, using criterion 3.

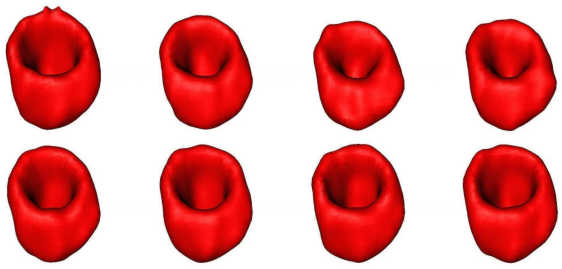

Fig. 6. From left to right and top to bottom, segmentation results from frame 0 to frame 7 of the cardiac sequence, using criterion 5.

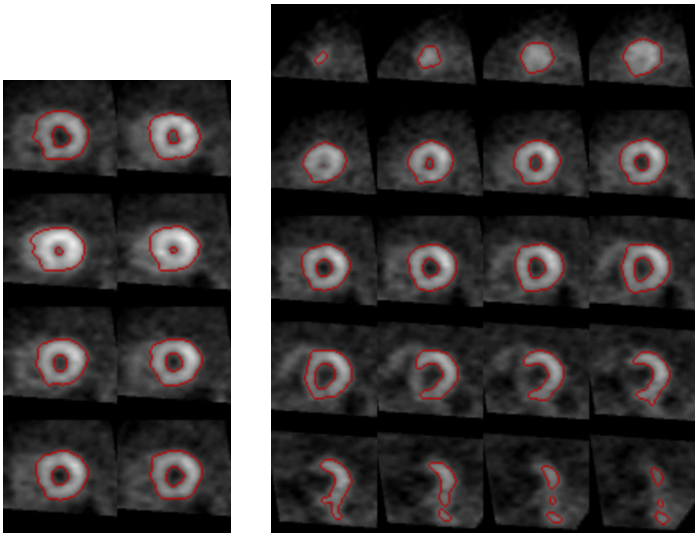

Fig. 7. On the left, the whole cardiac sequence viewing plane Z=11 with segmentation result superimposed (using criterion 3). On the right, data of frame 6 with segmentation result superimposed. We observe the two stages of a heart beat : the systole (frames 1 to 3) and the diastole (frames 4 to 7 and 0).

8 Discussion and perspectives

In this study, we have improved the segmentation (i) in quality by improving the robustness to noise and (ii) in time: we have reduced the total algorithm time by 85%. We have studied in details each step of the algorithm. Various parameters such as the reinitialization frequency or the curvature weight were analyzed and tuned for reducing the computation time to a minimum.

This study of the mathematical parameters now need to be further investigated on clinical data. A more thorough validation involving comparison to segmentation results by medical experts on a larger dataset is needed. Additional constraints taking into account the physiology of the heart such as the almost incompressibility of the muscle could also be implemented. The method could then be used to extract quantitative functional parameters.

Aknowkedgments : The authors would like to thank Pr. J. Darcourt for fruitful discussions.

This work is partly financed by the CNRS (French National Center for Scientific Research) STIC department as a multilaboratory Project (Creatis in Lyon, I3S in Sophia Antipolis and Pasteur Hospital in Nice)"

References

1. V. Caselles, F. Catte, T. Coll, and F. Dibos. A geometric model for active contours in image processing. In *Numerische Mathematik*, volume 66, pages 1–33, 1993.
2. V. Caselles, R. Kimmel, and G. Sapiro. Geodesic active contours. *International Journal of Computer Vision*, 22(1):61–79, 1997.
3. L.D. Cohen and Isaac Cohen. Finite element methods for active contour models and balloons for 2-D and 3-D images. *IEEE Transactions on Pattern Analysis and Machine Intelligence, PAMI*, 15, November 1993.
4. L.D. Cohen and Ron Kimmel. Global minimum for active contour models: A minimal path approach. *Int. J. of Computer Vision*, 24(1):57–78, 1997.
5. E. Debreuve, M. Barlaud, G. Aubert, I. Laurette, and J. Darcourt. Space time segmentation using level set active contours applied to myocardial gated spect. In *International Conference on Medical Imaging (MIC99), Vancouver*, Octobre 1999.
6. J. Gomes and O.D. Faugeras. Reconciling Distance Functions and Level Sets. *Journal of Visual Communication and Image Representation*, 11:209–223, 2000.
7. S. Jehan-Besson, M. Barlaud, and G. Aubert. A 3-step algorithm using region-based active contours for video objects detection. *EURASIP Journal of Applied Signal Processing*, 2002(6):572–581, 2002.
8. M. Kass, A. Witkin, and D. Terzopoulos. SNAKES: Active contour models. *International Journal of Computer Vision*, 1:321–332, January 1988.
9. R. Malladi, J. A. Sethian, and B.C. Vemuri. Shape modeling with front propagation: A level set approach. *IEEE Transactions on Pattern Analysis and Machine Intelligence*, 17(2):158–175, February 1995.
10. J. Montagnat and H. Delingette. A review of deformable surfaces: topology, geometry and deformation. *Image and Vision Comput.*, 19(14):1023–1040, Dec. 2001.
11. S. Osher and J. Sethian. Fronts propagating with curvature dependent speed : algorithms based on the Hamilton-Jacobi formulation. *Journal of Computational Physics*, 79:12–49, 1988.
12. Nikos Paragios and Rachid Deriche. Geodesic active contours and level sets for the detection and tracking of moving objects. *IEEE Transactions on Pattern Analysis and Machine Intelligence*, 22(3):266–280, March 2000.
13. P.H. Pretorius, W. Xia, M. A. King, B. M. W. Tsui, T.-S. Pan, and B.J. Villegas. Determination of left and right ventricular volume and ejection fraction using a mathematical cardiac torso phantom for gated blood pool spect. *Journal of Nuclear Medicine*, 37:97, 1996.
14. M. Sussman, P. Smereka, and S. Osher. A level set approach for computing solutions to incompressible two-phase flow. *J. Comput. Physics*, 114:146–159, 1994.
15. D. Terzopoulos, A. Witkin, and M. Kass. Constraints on deformable models : Recovering 3d shape and non rigid motion. *Artificial Intelligence*, 36(1):91–123, 1988.